Supplementary Information for

Common dynamical features of sensory adaptation in photoreceptors and olfactory sensory neurons

G. De Palo[†], G. Facchetti[†], M. Mazzolini[†‡], A Menini[†], V. Torre[†‡] and C. Altafini[†]
[†]SISSA, International School for Advanced Studies,
via Bonomea 265, 34136 Trieste, Italy,
[‡]CBM (Consorzio di Biomedicina Molecolare)
Area Science Park, Basovizza, 34149 Trieste, Italy altafini@sissa.it

Contents

1 Further considerations on elementary 2-variable models

1.1 From exact integral feedback model to integral feedback with memory decay

This section is meant to explain why on elementary models a simple exact integral feedback is not suitable to reproduce the data analyzed in the paper. For the sake of simplicity, we take as reference the experiments with olfactory neurons shown in Fig. 2 of the paper, in which the input positively stimulates the state variable y of the system (and hence the output). We review (basic) models starting from the one in [31] and adding elements to it, with the aim of "qualitatively" satisfying the following dynamical features:

- reproduce the step adaptation of the paper, with its steady state value which is similar but not exactly equal to the pre-stimulus level;
- reproduce the two-pulse adaptation protocol shown in the paper, with its recovery profile;
- avoid non-physiological signals. These correspond for example to negative concentrations of a substance, but also to unrealistic transient excursions. In particular in all our experimental data for olfactory response (see [9]), the output current never undershoots the basal level of current, neither in a step adaptation nor in a multipulse protocol.

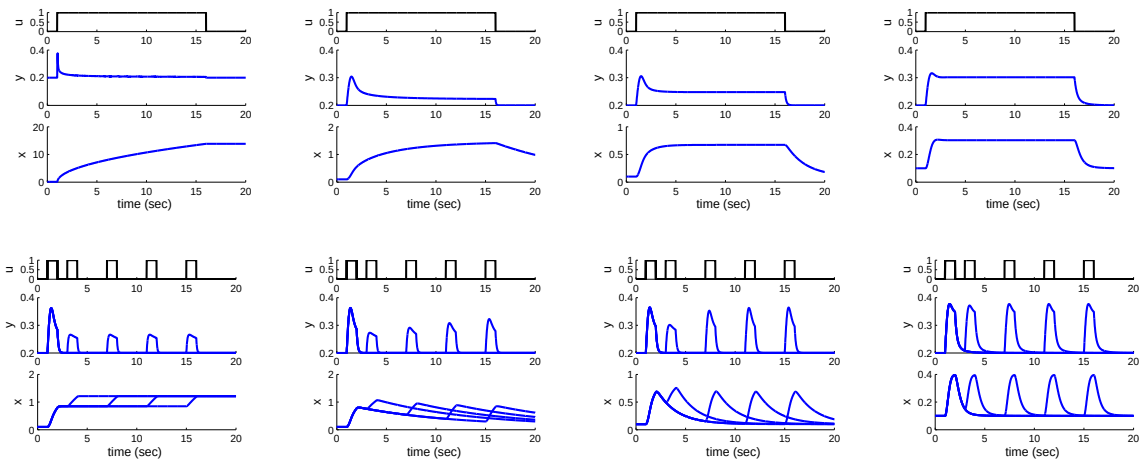

Figure S1: **Input responses of the 2-variable model** (1) **of the paper.** The various plots of Fig. 1B of the paper are shown here more in detail. The 4 panels show the time course of the input (u) and state variables (y and x) of model (1) of the paper in response to steps (top) and multiple pulse pairs (bottom) for 4 different values of the ratio δ_y/δ_x. The same classification as in Fig. 1B is followed. A: perfect step adaptation / no recovery in multipulse adaptation; B: almost perfect step adaptation / slow recovery in multipulse adaptation; C: partial step adaptation / fast recovery in multipulse adaptation; D: no step adaptation / no multipulse adaptation.

Model 1. The basic integral feedback model. Following the notation of the caption of Fig. 2 of [31], the basic model is

$$y = k_1(u - x) - y_o \tag{S1a}$$

$$\frac{dx}{dt} = y, \tag{S1b}$$

where y is the output variable, y_o its basal level, and x the feedback variable.

A characteristic of this model is that when $y \geq 0 \ \forall t \geq 0$ (physiological condition for most biological models, including ours) $x(t) = \int_0^t y(\tau)d\tau$ is monotonically growing. Hence no matter how delayed is the second pulse of a two-pulse protocol, $y(t) \geqslant 0$ implies $x(t_2) \geqslant x(t_1) \ \forall t_2 > t_1$, meaning that the adapted response does not recover increasing the lag time between the two pulses. The only way to decrease x (to "discharge" the integrator in control engineering language) is to allow for negative y, see Fig. S2. Notice that the model is exactly the same as the following one, with baseline "shifted"

$$y = k_1(u - x)$$

$$\frac{dx}{dt} = (y - y_o),$$

where integration is with respect to the baseline value y_o. Now the output y "moves around" y_o, hence when $y_o > 0$ it could remain positive even if $y - y_o < 0$. However, in the multipulse response the problem of possible negative values of y reappears if the amplitude of u is increased, meaning the model is not structurally consistent for biological signals. Furthermore, the profile for the deactivation phase (following the end of a pulse)

is not physiological, and differs from any experimentally observed profile. More comments on this in next subsection.

In addition, y has jumps when u has jumps, since (S1a) is a static input-output relationship.

Model 2. Adding a kinetics to the input-output relationship. The static input-output transduction of Eq. (S1a) can be replaced by a differential equation, describing the kinetics from input u to output y

$$\frac{dy}{dt} = f(u, x) \tag{S2a}$$
$$\frac{dx}{dt} = y, \tag{S2b}$$

where $f(\cdot)$ is any kinetic function, for example a linear one: $f(u, x) = u - k_1 x$.

In this way we obtain a linear system $\xi = \begin{bmatrix} y \\ x \end{bmatrix}$

$$\frac{d\xi}{dt} = A\xi + Bu,$$

where $A = \begin{bmatrix} 0 & -k_1 \\ 1 & 0 \end{bmatrix}$, $B = \begin{bmatrix} 1 \\ 0 \end{bmatrix}$. A system like this is not asymptotically stable ($\text{trace}(A) = 0$ means the eigenvalues are purely imaginary) and typically induces oscillations in response to steps, see Fig. S2. However if we add a damping, i.e., a negative term on the diagonal of A, then asymptotic stability is recovered.

Model 3. Adding a damping term to the y equation. A first possibility is to place the damping term (a first order decay) in the input-output transduction:

$$\frac{dy}{dt} = u - k_1 x - \delta_y y \tag{S3a}$$
$$\frac{dx}{dt} = y, \tag{S3b}$$

or, in presence of a nonzero baseline y_o,

$$\frac{dy}{dt} = u - k_1 x - \delta_y y \tag{S4a}$$
$$\frac{dx}{dt} = y - y_o. \tag{S4b}$$

From Fig. S2, these curves are qualitatively correct for double pulse adaptation and show perfect step adaptation. However, as in **Model 1** the double pulse adaptation is obtained only because y becomes negative (or undershoots its baseline), hence the model is inadequate for the same reasons.

In order to avoid negative values of y, the simplest solution is to introduce a nonlinearity in the ODE for y, for example a quadratic term, in our case representing the "encounters" of x and y in a mass-action formalism.

Model 4. Adding a quadratic term on **Model 3**. Adding the quadratic term in the input-output transduction and keeping the linear decay in y we get

$$\frac{dy}{dt} = u - k_1 xy - \delta_y y \tag{S5a}$$
$$\frac{dx}{dt} = y. \tag{S5b}$$

From Fig. S3, the model (S5)

- avoids negative values for y;
- does not reach a steady state in x in the step response ($dx/dt > 0$ always);
- shows no recovery of the adaptation to a double pulse.

The latter item in particular is unavoidable regardless of the functional form chosen for the kinetics of y, as long as the exact integral ODE (S5b) is used. In this case in fact the only way to "discharge" the integrator is when y assumes negative values.

We deduce therefore that adaptation to a double pulse cannot be achieved by an exact integral feedback in which the integrated variable is never negative. The argument is similar in presence of a baseline y_o (and of an output y s.t. $y - y_o \geq 0$ always, as in our experiments).

Model 5. Quadratic term as in **Model 4** and damped integral feedback.

In this model the diagonal damping term affects the feedback variable:

$$\frac{dy}{dt} = u - k_1 xy \tag{S6a}$$
$$\frac{dx}{dt} = y - \delta_x x. \tag{S6b}$$

This is the starting point of our scheme of an integral feedback with a memory decay, used in the paper.

From Fig. S3, the model (S6)

- avoids negative values of y (or of $y - y_o$ in case of nonzero baseline);
- shows a non perfect adaptation to a step;
- exhibits a recovery of the adaptation in a double pulse protocol.

Qualitatively this elementary model reproduces all the dynamical features observed in the experimental data described in the paper. The presence of a damping term $-\delta_y y$ in (S6a) does not alter this qualitative behavior provided that δ_x/δ_y is small enough (the time constant of x is longer than the one of y, see main text).

Model 6. Adding a conservation law to **Model 5**.

If, as in our models, y represents a fraction of a certain molecular species of constant total concentration (e.g. the fraction of open CNG channels in olfactory transduction), then its value must be constrained, for example assuming $0 \leqslant y \leqslant 1$. The **Models 1÷5** do not respect this constraint, because u is not linked to the value assumed by y. A conservation

law can be imposed multiplying u by the complement of y (i.e., by the fraction of closed CNG channels in the olfactory pathway). The resulting model

$$\frac{dy}{dt} = u(1-y) - k_1 xy \tag{S7a}$$

$$\frac{dx}{dt} = y - \delta_x x, \tag{S7b}$$

is the one used in the paper once a degradation term is added in (S7a). A similar conservation law can in principle be applied also to x (not necessary in our case). As can be seen on Fig. S3, the behavior of **Model 6** is qualitatively similar to that of **Model 5** for what concerns our input responses.

Whenever basal regulation is nonnegligible, nonzero baseline levels can be taken into account for both y (as we did above with y_o) and x (denote it x_o). The model (S7) can be amended as follows:

$$\frac{dy}{dt} = u(1-y) - k_1(x-x_b)(y-y_o) \tag{S8a}$$

$$\frac{dx}{dt} = (y-y_o) - \delta_x(x-x_o) \tag{S8b}$$

where the baseline may or may not be present in the first order degradation rates, depending on the context.

1.2 "Discharging" an integral feedback by undershooting: confutation of an alternative model.

Reviewing the behavior of the basic **Models 1** through **5** of the previous section, it can be observed that even with an integral feedback it is possible to generate output profiles which match qualitatively the responses to both types of adaptation but do not exhibit the trade-off mentioned in the paper. This case corresponds for example to Model 3 of this SI, see (S3) and Fig. S2. In this model, the (exact) integrator is "discharged" through a signal that undershoots the baseline level, avoiding any memory decay. From (S4) if y_o is the baseline of y, then $y < y_o$ implies that even with $\delta_x = 0$ the integral $x(t) = \int_0^t (y(\tau) - y_o)d\tau$ is no longer monotone, i.e., the integral $x(t)$ can indeed decrease also in a model with exact integral feedback.

The undershooting in the deactivation phase should however be observable experimentally, i.e., it should produce an output current which becomes less than basal in olfactory transduction or higher than basal in phototransduction. No experiment with the olfactory system shows undershooting of the basal current. Also in phototransduction experiments, for both pulse and step responses in dark, no overshooting above the noise level can be observed in the deactivation phase. For both sensors, a large number of similar experiments available in the literature confirms the lack of undershoot (overshooting for phototransduction) deactivation transients [2, 12, 25, 6, 13, 22].

Furthermore, if y represents a fraction of a (positive) quantity, $0 \leqslant y,\ y_o \leqslant 1$, the scheme making use of undershooting to discharge the integral, in order to be plausible, requires that y_o is sufficiently large. In olfactory transduction, however, y reflects the fraction of open CNG channels, and it is estimated that $y_o \sim 0$ in absence of stimulation (y reaches 0.9 upon strong stimulations). Hence, to preserve nonnegativity of concentrations, the admissible undershooting would in any case be extremely limited. The behavior in phototransduction is not completely specular, in the sense that, for the "complementary variable" $z = 1-y$, z_o (representing the basal fraction of open channels) in dark is low, and during the transient it decreases further, $z \leqslant z_o$

Model 1

$$\begin{aligned} y &= k_1(u-x) \\ \frac{dx}{dt} &= y \end{aligned}$$

exact integral feedback
static input-output map
undershooting

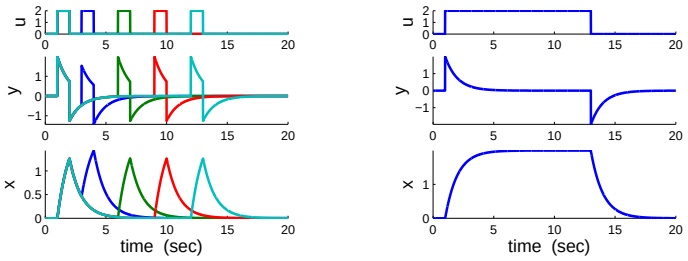

Model 2

$$\begin{aligned} \frac{dy}{dt} &= u - k_1 x \\ \frac{dx}{dt} &= y \end{aligned}$$

exact integral feedback
not asymptotically stable

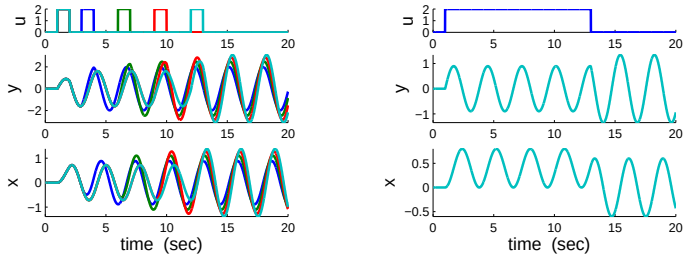

Model 3

$$\begin{aligned} \frac{dy}{dt} &= u - k_1 x - \delta_y y \\ \frac{dx}{dt} &= y \end{aligned}$$

exact integral feedback
asymptotically stable
undershooting

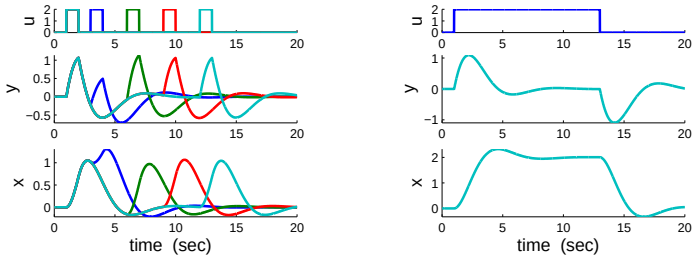

Figure S2: **Step and multipulse response for the Models 1-3**. The main dynamical properties of the models are summarized below the equation box.

(i.e., CNG channels close even more, up to a complete closure for saturating illuminations). In spite of this, it is worth observing that when stimulated in dark, overshooting transients in the deactivation phase of a pulse/step are not seen in experiments with rods.

The similarity of the behavior in the two sensors confirms that "discharging" of the feedback variable(s) has to be accomplished by some other mechanism such as the memory decay described in the paper. Other pieces of evidence in favor of the memory decay mechanism include the graded steady state level reached in response to graded step inputs, see [9] for a relate discussion in the olfactory transduction system. Remarkably for cones (which are known to never saturate [23]) some form of undershooting is instead observed [16].

Model 4

$$\begin{aligned} \frac{dy}{dt} &= u - k_1 xy - \delta_y y \\ \frac{dx}{dt} &= y \end{aligned}$$

exact (bilinear) integral feedback
never undershooting
no multipulse adaptation
no steady state for step adaptation

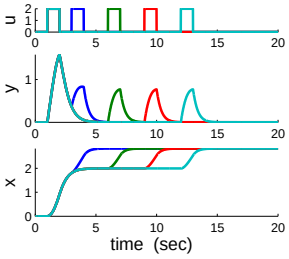

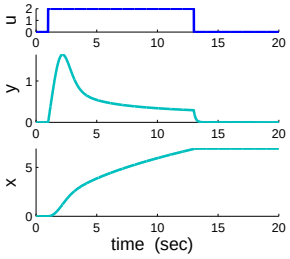

Model 5

$$\begin{aligned} \frac{dy}{dt} &= u - k_1 xy \\ \frac{dx}{dt} &= y - \delta_x x \end{aligned}$$

integral feedback with memory decay
never undershooting
multipulse adaptation
(non-perfect) step adaptation

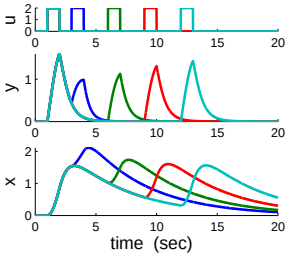

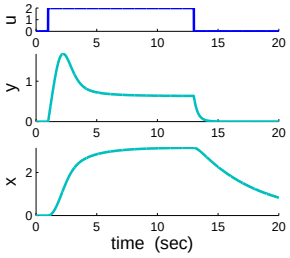

Model 6

$$\begin{aligned} \frac{dy}{dt} &= u(1-y) - k_1 xy \\ \frac{dx}{dt} &= y - \delta_x x \end{aligned}$$

conservation law for y
integral feedback with memory decay
never undershooting
multipulse adaptation
(non-perfect) step adaptation

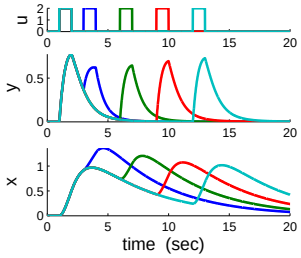

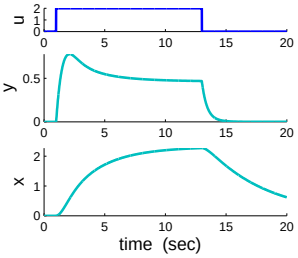

Figure S3: **Step and multipulse response for the Models 4-6**. The main dynamical properties of the models are summarized below the equation box.

2 Signaling pathways and their models

2.1 Olfactory transduction

Pathway. In the absence of stimuli, the cyclic nucleotide-gated (CNG) channels in the olfactory transduction are almost completely closed. The arrival of the odorant molecules increases, through a G-protein cascade, the amount of activated adenylyl cyclase, which in turn leads to the accumulation of cyclic AMP, thus triggering the opening of the CNG channels. This allows various types of cations to enter the cell. Among these, the calcium ions further open the calcium-activated chloride channels, leading to a second current of chloride anions which flows out from the cell, amplifying the original response [15, 21]. Calcium is also responsible for several feedback loops in the pathway: by binding to proteins (among these possibly calmodulin)

which are natively attached to the CNG channels, it decreases the sensitivity of the channels to cAMP thus inducing their closure [1, 5, 8]. Furthermore, by binding to calmodulin free in the cytoplasm it causes the hydrolysis of cAMP through a phosphodiesterase (PDE) [4], and this calcium-calmodulin (CaCaM) complex can activate also the enzyme CaCaM-dependent protein kinase II (CaMK) which inhibits the adenylyl cyclase activity [29]. Calcium is finally extruded through the Na/Ca exchanger [20]. More details on the pathway are available e.g. in [15, 2].

Dynamical model. For the sake of simplicity, these feedback actions are lumped together into the single feedback shown in Fig. S4A. Extensive analysis of more complex models carried out in [9] in fact suggests that the multiple feedback actions are redundant for what concerns the adaptation behavior considered in this paper. Our "minimal" model includes therefore 3 state variables: [CNG] (fraction of open channels), [Ca] (concentration of Ca^{2+} ions) and [CaBP] (concentration of the complexes that calcium forms with the protein complexes natively bound to the CNG channels, here indicated as BP). The first and the latter of these variables obey a conservation law. The total number of CNG channels (normalized to one) is the sum of the closed and the open channels (respectively $[\mathrm{CNG}_c]$ and [CNG]). Furthermore the equation $[\mathrm{BP}]+[\mathrm{CaBP}]=1$ represents the conservation of the total concentration of the calcium-binding proteins BP. For this reaction a mass-action kinetic is considered:

$$\mathrm{Ca}^{2+} + \mathrm{BP} \underset{\beta_{\mathrm{CaBP}}}{\overset{\alpha_{\mathrm{CaBP}}}{\rightleftharpoons}} \mathrm{CaBP}.$$

In our dynamical model the cyclic AMP can be considered as the input of the system (here called u):

$$\frac{\mathrm{d}[\mathrm{CNG}]}{\mathrm{dt}} = (1-[\mathrm{CNG}])u - k_1[\mathrm{CNG}][\mathrm{CaBP}]^2 \tag{S9a}$$

$$\begin{aligned}\frac{d[\mathrm{Ca}]}{dt} &= k_2[\mathrm{CNG}] - \delta_{\mathrm{Ca}}[\mathrm{Ca}] \\ &\quad -\alpha_{\mathrm{CaBP}}[\mathrm{Ca}](1-[\mathrm{CaBP}]) + \beta_{\mathrm{CaBP}}[\mathrm{CaBP}]\end{aligned} \tag{S9b}$$

$$\frac{d[\mathrm{CaBP}]}{dt} = \alpha_{\mathrm{CaBP}}[\mathrm{Ca}](1-[\mathrm{CaBP}]) - \beta_{\mathrm{CaBP}}[\mathrm{CaBP}]. \tag{S9c}$$

In (S9a) the first term represents the opening of the CNG channels due to cyclic AMP and the second term the negative feedback (which includes a cooperative action, known to hold for calmodulin [5]). Equations S9b and S9c include the mass-action terms introduced above and the inflow of calcium due to the opening of the channels (term $k_2[\mathrm{CNG}]$). The linear degradation term $\delta_{\mathrm{Ca}}[\mathrm{Ca}]$ includes also the extrusion of calcium through the sodium-calcium exchanger. More details on the kinetic terms are available on [9].

In the cilia the CNG current is further amplified by the chloride current flowing through the calcium-activated chloride channels. Therefore the output of our model (total elicited current) is calculated as the sum of the current flowing through the CNG channels (proportional to the fraction of open channels), and of that carried by chloride anions. To account for this second component we use a Hill-dependence on the calcium concentration with a cooperativity index n equal to 2 (as in [15, 2, 28]) and with the half-activation constant $K_{1/2}$ equal to 4 μM [15, 2, 9]. Furthermore we have added a weight of 0.2 for the current carried by CNG channels and of 0.8 for the calcium-activated chloride current, to reflect their proportionality in the biological data [3]

$$I_{\mathrm{olf}} = 0.2\,[\mathrm{CNG}] + 0.8\Big(\frac{[\mathrm{Ca}]^n}{[\mathrm{Ca}]^n + K_{1/2}^n}\Big). \tag{S10}$$

2.2 Phototransduction

The signaling mechanisms involved in the phototransduction of vertebrate rods are described at length in several survey papers, such as [6, 11, 23, 22]. Also several detailed mathematical models exist, see e.g. [13, 14, 22, 27]. Coherently with the approach followed in this paper, only the basic ingredients needed to have a minimal regulatory system are considered in our model.

Pathway. In darkness, rods are characterized by Ca^{2+} and Na^{+} currents which circulate through cGMP-gated CNG channels (inflow) and exchange pumps (outflow). Light photoisomerizes rhodopsin which, through the mediation of G-proteins, activates PDE. Activated PDEs hydrolize cGMP, and the drop of cGMP induces the closure of the CNG channels and hence a drop in the Ca^{2+} current. As the efflux through the exchange pumps is not affected, also the cytoplasmic concentration of Ca^{2+} drops. In dark, Ca^{2+} binds to the guanylate cyclase activating protein (GCAP) reducing its function of inhibitor of guanylate cyclase (GC) activity. The drop of Ca^{2+} during light response implies calcium-free GCAP binds to GC and increases its catalytic activity for second messengers. Hence the synthesis of cGMP passes from a basal level to a higher rate, thereby completing the negative feedback loop which forms the core of the regulation considered in our model. Calcium is responsible for at least two more feedback mechanisms present in the phototransduction pathway[1]. It decreases the affinity of CNG channels through the binding with calmodulin, and the calcium-binding protein recoverin inhibits the phosphorilation of rhodopsin due to G-protein-coupled-receptor-kinase 1 (GRK1) preventing the complete deactivation of rhodopsin by arrestin. Therefore, a decreasing concentration of calcium promotes the activity of GC, the opening of the CNG channels and the quench of rhodopsin [22, 18, 30]. The feedback involving the modulation of the GC is considered dominant at low and intermediate light intensities, whereas the feedback due to recoverin-arrestin seems to play a more important role at higher intensities [30]. The feedback action of calcium ions on CNG-channels is of little importance in rods phototransduction compared with the other two mechanisms [17].

Dynamical model. In what follows we will disregard the feedbacks mediated by calmodulin and by recoverin and concentrate on the GC feedback loop. The resulting basic pathway considered in our model is depicted in Fig. S5A. For this pathway we consider a model of 4 variables: [cGMP] (concentration of cGMP), [CNG] (fraction of open CNG channels), [Ca] (concentration of Ca^{2+} ions), [GC] (fraction of active guanylate cyclase). GCAP is not modeled explicitly. Conservation laws are imposed on [CNG] and [GC]. Denoting $[CNG_c]$ and $[GC_i]$ respectively the fraction of closed CNG channels and the fraction of inactive GC enzyme, these conservation laws can be expressed as $[CNG]+[CNG_c]=1$ and $[GC]+[GC_i]=1$. The reactions for which we use mass-action kinetics are the following:

$$
\begin{aligned}
CNG_c + 2cGMP &\underset{\beta_{CNG}}{\overset{\alpha_{CNG}}{\rightleftharpoons}} CNG \\
GC + 2Ca^{2+} &\underset{\beta_{GC}}{\overset{\alpha_{Ca}}{\rightleftharpoons}} GC_i \\
cGMP &\xrightarrow{\delta_{CNG}} \emptyset \quad \text{(hydrolized to GMP)} \\
Ca^{2+} &\xrightarrow{\delta_{Ca}} \emptyset \quad \text{(outflow from the outer segment).}
\end{aligned}
$$

The second reaction models the (GCAP mediated) inhibition of GC by Ca^{2+}, which occurs in darkness. Additional (non-mass action) reactions express the inflow of Ca^{2+} through the open

[1] Several extra feedback loops are actually mentioned in [22] but will not be described here.

CNG channels (linear term, with gain constant k_2), and the feedback action (linear production of cGMP, whose substrate, GTP, is considered abundant). The ODEs we will use are the following:

$$\begin{aligned}
\frac{d[\mathrm{cGMP}]}{dt} &= -(u+\delta_{\mathrm{cGMP}})[\mathrm{cGMP}] + k_1[\mathrm{GC}] \\
&\quad -2\alpha_{\mathrm{CNG}}[\mathrm{cGMP}]^2(1-[\mathrm{CNG}]) + 2\beta_{\mathrm{CNG}}[\mathrm{CNG}] && \text{(S11a)} \\
\frac{d[\mathrm{CNG}]}{dt} &= \alpha_{\mathrm{CNG}}[\mathrm{cGMP}]^2(1-[\mathrm{CNG}]) - \beta_{\mathrm{CNG}}[\mathrm{CNG}] && \text{(S11b)} \\
\frac{d[\mathrm{Ca}]}{dt} &= k_2[\mathrm{CNG}] - \delta_{\mathrm{Ca}}[\mathrm{Ca}] - 2\alpha_{\mathrm{GC}}[\mathrm{GC}][\mathrm{Ca}]^2 + 2\beta_{\mathrm{GC}}(1-[\mathrm{GC}]) && \text{(S11c)} \\
\frac{d[\mathrm{GC}]}{dt} &= -\alpha_{\mathrm{GC}}[\mathrm{GC}][\mathrm{Ca}]^2 + \beta_{\mathrm{GC}}(1-[\mathrm{GC}]) && \text{(S11d)}
\end{aligned}$$

In the phototransduction experiments the only affected current in response to light stimuli is the one flowing through the CNG channels. Therefore the output of the model (reproducing the measured current) is considered proportional to the fraction of open CNG channels. To account for the normalization and the shift of the recorded currents (otherwise impossible to compare because of the different amplitudes and responses) we inserted in the model two parameters: K_I representing the amplification of the current and I_0 to account for a different dark current level:

$$I_{\mathrm{photo}} = I_0 + K_I[\mathrm{CNG}]. \tag{S12}$$

2.3 Parameter fitting

Modeling the input stimulus. For phototransduction, the input of our model is the PDE which hydrolyzes the cGMP. Since we do not describe the early steps of the pathway, the dynamics of activation is taken from literature. For instance, the tailed peak of PDE from a pulse stimuli reported in [24] is here reproduced (normalized) with the following expression

$$u(t) = \begin{cases} 0 & t < t_o \\ (t-t_o)\lambda e^{1-\lambda(t-t_o)} & t \geqslant t_o \end{cases} \tag{S13}$$

where the parameter $\lambda = 6.0$. Step inputs are reproduced holding the maximum value of this function for the whole length of the pulse. Moreover, we assume that the stronger action induced by a step (with respect to a short pulse) reflects also in a slower decay. In these cases the parameter λ is reduced to 2.2. The same input modeling is used for the olfactory transduction, with values of $\lambda = 2$ and $\lambda = 1$ respectively.

Fitting procedure. The parameters of the models (S9) and (S11) have been fitted to the data presented in Figs. 2 and 3-4 of the main text. To perform this fit, we used the MATLAB function lsqcurvefit. This function minimizes the residuals sum of squares of the different datasets simultaneously with a nonlinear least square method (using the trust-region-reflective algorithm). The resulting values of the parameters are reported in Tables S1 and S2.

Inducing adaptation via negative feedback: faster and slower time constants. As mentioned in the main text, if in a model like (1) exact integral feedback implies an infinite time constant for the variable x, achieving partial step adaptation still requires a system with a faster (y) and a slower (x) kinetics, see Fig. S1. Also the models (S9) and (S11) obey this principle.

Name	Description	Value
k_1	CaBP feedback gain	215
k_2	inflow of Ca^{2+} through CNG channels	23
δ_{Ca}	outflow of Ca^{2+}	1.5
α_{CaBP}	association rate between Ca^{2+} and BP	0.10
β_{CaBP}	dissociation rate between Ca^{2+} and BP	0.21

Table S1: **Parameter set used to fit the olfactory transduction data of Fig. 2.**

Name	Description	Value
δ_{cGMP}	degradation rate of cGMP	0.38
k_1	GC feedback gain	3480
α_{CNG}	association rate between CNG and cGMP	1.95
β_{CNG}	dissociation rate between CNG and cGMP	150
k_2	inflow of Ca^{2+} through CNG channels	440
δ_{Ca}	outflow of Ca^{2+}	28
α_{GC}	association rate between Ca^{2+} and GC	0.10
β_{GC}	dissociation rate between Ca^{2+} and GC	0.0018

Table S2: **Parameter set used to fit the phototransduction data of Figs. 3-4.**

For example, it is known that in phototransduction the opening and closing of the CNG channels occurs on a very fast time scale (milliseconds, [22]) when compared with the PDE-mediated decline of the input stimulus and with the regulatory action of GC, which is induced by GCAP reactivation following the Ca^{2+} drop. Therefore for the purposes of our modeling we can consider the CNG gating (and the consequent kinetics of Ca^{2+} influx/efflux) as faster processes when compared to the negative feedback regulation due to GC, see Fig. S5A.

Similarly in the olfactory transduction, the time constant of the feedback mechanism is longer than that associated with the opening of the CNG channels. As just mentioned, this last is known to be very fast, of the order of milliseconds, while the onset of the feedback is neatly slower, as can be seen in Fig. 2 of the paper. Notice that also in [9], where related models are studied in detail, similar ranges of values for the time scales of the system emerge naturally when trying to fit step/multipulse response data.

Finally, it is worth remarking that the presence of fast and slow dynamics is a prerequisite also in other models for adaptation not discussed in this paper, like the incoherent feedforward loop (in this case a delay element is often used to mimic slower response).

On minimality of the model and identificability At the level of a single photoreceptor, much more detailed kinetic models than the one adopted here to fit the data have been available for several years [13, 22, 14, 27]. The same consideration applies also to the olfactory transduction [10, 9]. As we have recently observed for the latter pathway in [9], from the perspective of the input-output dynamical modeling (i.e., without the possibility of monitoring extra variables other than the stimulus and the output current) the introduction of extra details and of multiple feedback loops essentially introduces redundancy into the mathematical model. The complications associated with "non-minimal" dynamical models are well-known in the parameter identification literature [19, 26]. They essentially amount to the impossibility of uniquely determining the kinetic parameters of a model. The drastic choice made in this paper, namely to (deliberately) oversimplify the differential equations is also meant to avoid such type of ill-posed identifiability problems.

2.4 Response to a train of pulses: simulations

An intermediate situation between double pulse and step adaptation can be obtained through an input of consecutive pulses. When the lag time between the pulses is short, the stimulus obtained is similar to a step input. This protocol is sometimes used in experiments in alternative or in conjunction with steps, see e.g. [7]. The results of simulations with the models (S9) and (S11) of the two systems (see Figure S6) show an almost perfect adaptation for olfactory neurons and a very weak adaptation for photoreceptors. A comparison with the corresponding plots of a step input (panels B of Figure S4 and S5), highlights that the similarity concerns both the output and all the internal variables. For the stimulation of Fig. S6, the pulse width and the lag time reflect into the mean amplitude of the "effective" input (green curve), not in a substantial change of its functional form.

References

[1] S. Balasubramanian, J. W. Lynch, and P. H. Barry. Calcium-dependent modulation of the agonist affinity of the mammalian olfactory cyclic nucleotide-gated channel by calmodulin and a novel endogenous factor. *J Membr Biol*, 152(1):13–23, Jul 1996.

[2] A. Boccaccio, L. Lagostena, V. Hagen, and A. Menini. Fast adaptation in mouse olfactory sensory neurons does not require the activity of phosphodiesterase. *J Gen Physiol*, 128(2):171–184, Aug 2006.

[3] A. Boccaccio and A. Menini. Temporal development of cyclic nucleotide-gated and ca^{2+} -activated cl- currents in isolated mouse olfactory sensory neurons. *J Neurophysiol*, 98(1):153–160, Jul 2007.

[4] F. F. Borisy, G. V. Ronnett, A. M. Cunningham, D. Juilfs, J. Beavo, and S. H. Snyder. Calcium/calmodulin-activated phosphodiesterase expressed in olfactory receptor neurons. *J Neurosci*, 12(3):915–923, Mar 1992.

[5] J. Bradley, W. Bönigk, K. W. Yau, and S. Frings. Calmodulin permanently associates with rat olfactory CNG channels under native conditions. *Nat Neurosci*, 7(7):705–710, Jul 2004.

[6] M. E. Burns and D. A. Baylor. Activation, deactivation, and adaptation in vertebrate photoreceptor cells. *Annual Review of Neuroscience*, 24(1):779–805, 2001.

[7] L. Cervetto, V. Torre, E. Pasino, P. Marroni, and M. Capovilla. Recovery from light desensitization in toad rods. In A. Borsellino and L. Cervetto, editors, *Photoreceptors*, NATO-ASI, pages 159–175. Plenum Press, 1984.

[8] T. Y. Chen and K. W. Yau. Direct modulation by ca^{2+}-calmodulin of cyclic nucleotide-activated channel of rat olfactory receptor neurons. *Nature*, 368(6471):545–548, Apr 1994.

[9] G. De Palo, A. Boccaccio, A. Mirti, A. Menini, and C. Altafini. A dynamical feedback model for adaptation in the olfactory transduction pathway. *Biophysical J.*, 102(12):2677–2686, 2012.

[10] D. P. Dougherty, G. A. Wright, and A. C. Yew. Computational model of the cAMP-mediated sensory response and calcium-dependent adaptation in vertebrate olfactory receptor neurons. *Proceedings of the National Academy of Sciences of the United States of America*, 102(30):10415–10420, 2005.

[11] G. L. Fain, H. R. Matthews, M. C. Cornwall, and Y. Koutalos. Adaptation in vertebrate photoreceptors. *Physiological reviews*, 81(1):117–151, 2001.

[12] S. Firestein, G. M. Shepherd, and F. S. Werblin. Time course of the membrane current underlying sensory transduction in salamander olfactory receptor neurones. *J Physiol*, 430:135–158, Nov 1990.

[13] S. Forti, A. Menini, G. Rispoli, and V. Torre. Kinetics of phototransduction in retinal rods of the newt triturus cristatus. *J Physiol.*, 419:265–295, 1989.

[14] R. Hamer, S. Nicholas, D. Tranchina, T. Lamb, and J. Jarvinen. Toward a unified model of vertebrate rod phototransduction. *Vis Neurosci*, 22(4):417–36, 2005.

[15] S. J. Kleene. The electrochemical basis of odor transduction in vertebrate olfactory cilia. *Chemical Senses*, 33(9):839–859, 2008.

[16] J. I. Korenbrot. Speed, sensitivity, and stability of the light response in rod and cone photoreceptors: Facts and models. *Prog Retin Eye Res*, 31(5):442–466, Sep 2012.

[17] Y. Koutalos and K. W. Yau. Regulation of sensitivity in vertebrate rod photoreceptors by calcium. *Trends Neurosci*, 19(2):73–81, Feb 1996.

[18] D. Krizaj and D. R. Copenhagen. Calcium regulation in photoreceptors. *Front Biosci*, 7:2023–2044, Sep 2002.

[19] L. Ljung. *System identification: theory for the user*. Prentice Hall, Upper Saddle River, NJ, USA, 2nd edition, 1993.

[20] H. R. Matthews and J. Reisert. Calcium, the two-faced messenger of olfactory transduction and adaptation. *Current Opinion in Neurobiology*, 13(4):469 – 475, 2003.

[21] S. Pifferi, A. Boccaccio, and A. Menini. Cyclic nucleotide-gated ion channels in sensory transduction. *FEBS Lett*, 580(12):2853–2859, May 2006.

[22] E. Pugh Jr. and T. Lamb. Phototransduction in vertebrate rods and cones: Molecular mechanisms of amplification, recovery and light adaptation. In D. Stavenga, W. de Grip, and E. Pugh, editors, *Handbook of Biological Physics*, pages 183–255. Elsevier Science B.V., Amsterdam, 2000.

[23] E. Pugh Jr., S. Nikonov, and T. Lamb. Molecular mechanisms of vertebrate photoreceptor light adaptation. *Current Opinion in Neurobiology*, 9(4):410 – 418, 1999.

[24] J. Reingruber and D. Holcman. The dynamics of phosphodiesterase activation in rods and cones. *Biophysical journal*, 94(6):1954–1970, 2008.

[25] J. Reisert and H. R. Matthews. Adaptation-induced changes in sensitivity in frog olfactory receptor cells. *Chem Senses*, 25(4):483–486, Aug 2000.

[26] R. T. Roper, M. Pia Saccomani, and P. Vicini. Cellular signaling identifiability analysis: a case study. *J Theor Biol*, 264(2):528–537, 2010.

[27] L. Shen, G. Caruso, P. Bisegna, D. Andreucci, V. Gurevich, H. Hamm, and E. DiBenedetto. Dynamics of mouse rod phototransduction and its sensitivity to variation of key parameters. *IET Systems Biology*, 4(1):12–32, 2010.

[28] N. Suzuki, M. Takahata, and K. Sato. Oscillatory current responses of olfactory receptor neurons to odorants and computer simulation based on a cyclic AMP transduction model. *Chem. Senses*, 27(9):789–801, Nov 2002.

[29] J. Wei, A. Z. Zhao, G. C. Chan, L. P. Baker, S. Impey, J. A. Beavo, and D. R. Storm. Phosphorylation and inhibition of olfactory adenylyl cyclase by CaM kinase II in neurons: a mechanism for attenuation of olfactory signals. *Neuron*, 21(3):495–504, Sep 1998.

[30] K. W. Yau and R. C. Hardie. Phototransduction motifs and variations. *Cell*, 139(2):246–264, Oct 2009.

[31] T. M. Yi, Y. Huang, M. I. Simon, and J. Doyle. Robust perfect adaptation in bacterial chemotaxis through integral feedback control. *Proc. Natl. Acad. Sci. U.S.A.*, 97(9):4649–4653, 2000.

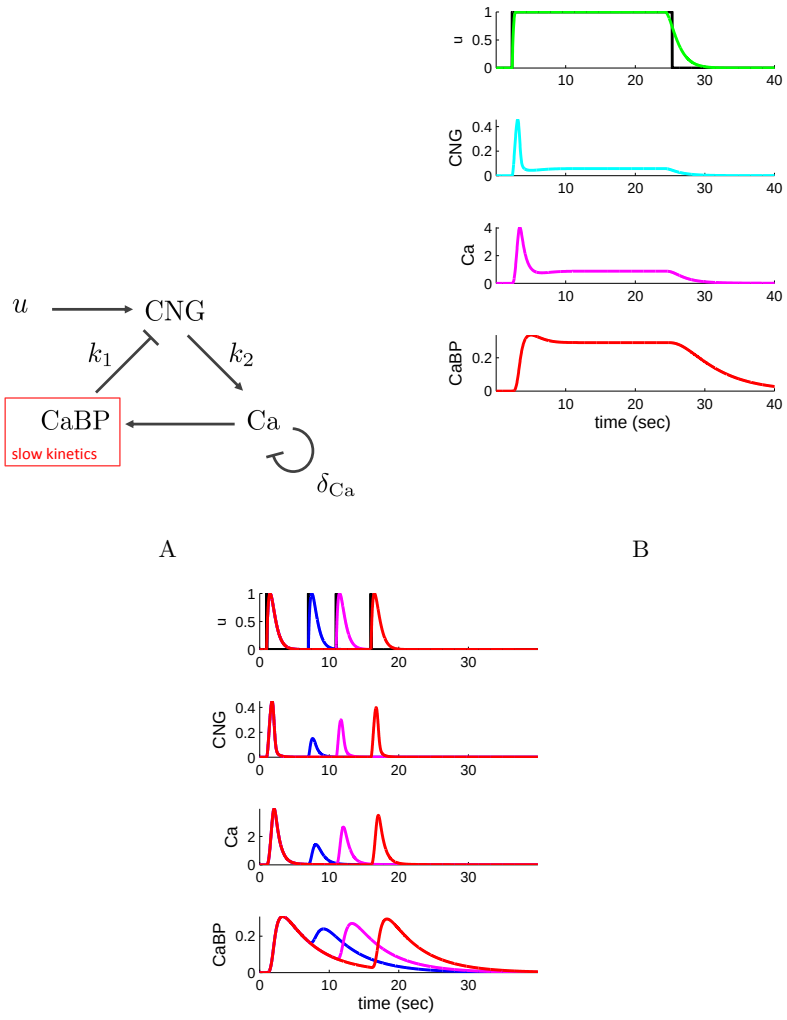

Figure S4: **Olfactory transduction.** A: the diagram represents the core regulatory action included in the model (S9) for the olfactory transduction, described in these SI. B: behavior of the state variables of (S9) for the step response of Fig. 2A of the paper. The top panel shows in black the "ideal" input and in green the more plausible input shape as described in (S13). C: state variables (and input) for the pulse pairs of Fig. 2B.

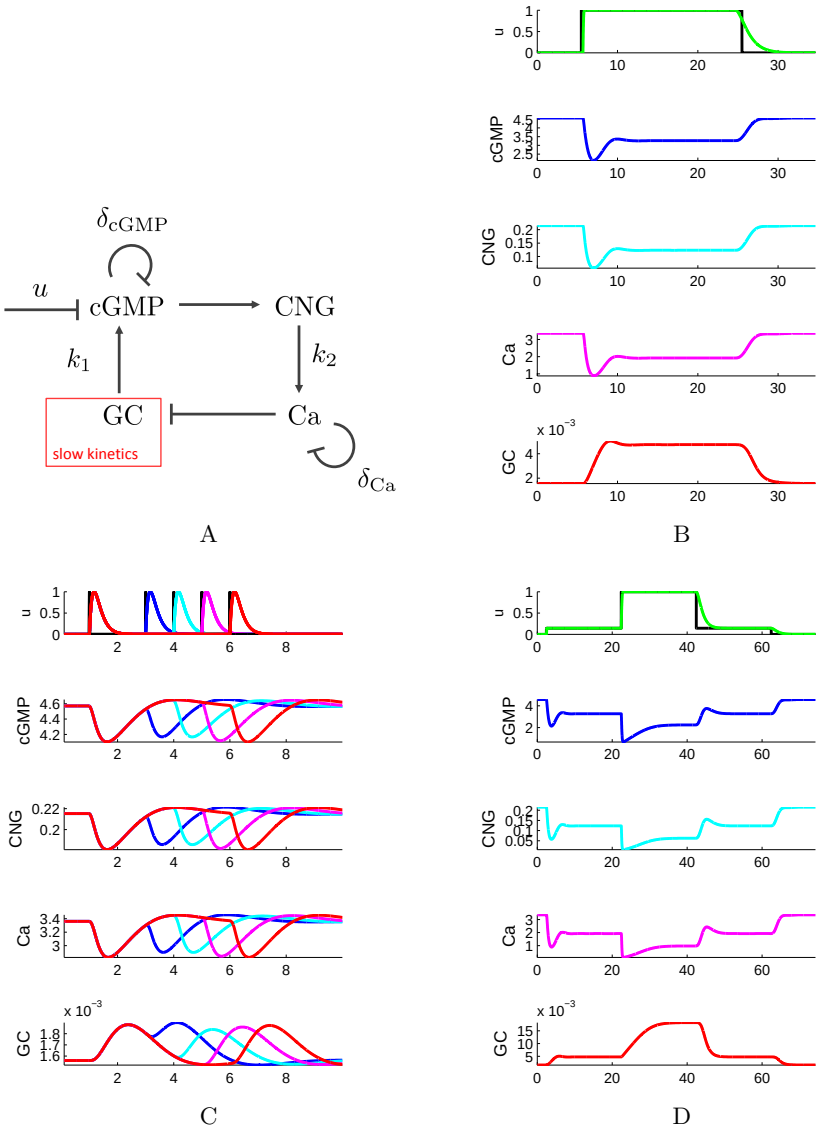

Figure S5: **Phototransduction.** A: the diagram shows the pathway used for phototransduction with its calcium-mediated GC feedback loop, see text and (S11). The panels B, C and D show the input u (both the ideal profile in black and the more realistic shape obtained from (S13) in color) and the 4 state variables of the model (S11) for B: the step response of Fig. 3A; C: the multipulse response of Fig. 3B; and D: the double step response of Fig. 4B.

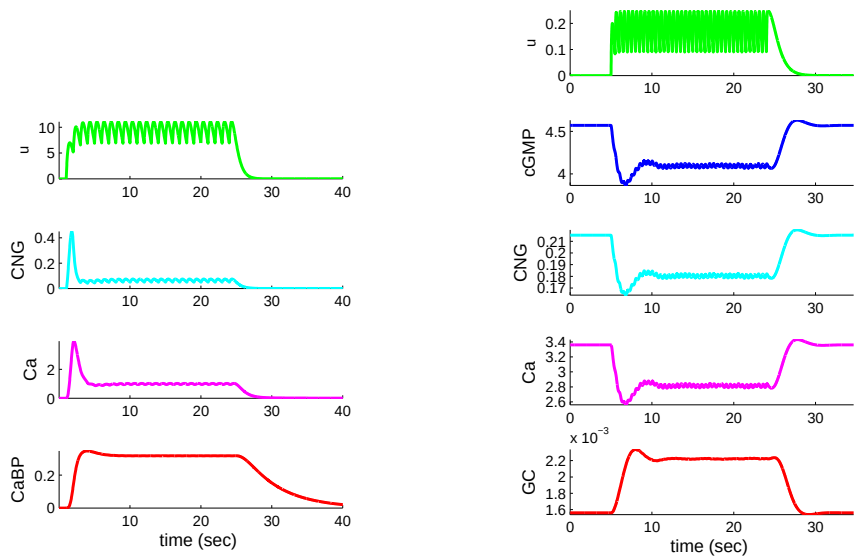

A B

Figure S6: **Response to a train of equispaced pulses.** The plots show the shaped input (green) and the state variables of both models (S9) and (S11) (panel A a B respectively) in response to consecutive equispaced ideal pulses u. Notice the similarity with step responses in Figure S4B and S5B.